Luminescence Characteristics of Terrestrial Jarosite from Kachchh, India: A Martian Analogue

Malika Singhal[1,2], Himela Moitra[3], Souvik Mitra[4], Aurovinda Panda[5], Jayant Kumar Yadav[5], D. Srinivasa Sarma[5], Devender Kumar[5], Naveen Chauhan[1], Saibal Gupta[3], Ashok Kumar Singhvi[1]

[1]Atomic and Molecular Physics Division, Physical Research Laboratory, Ahmedabad, 380009, India
[2] Indian Institute of Technology, Gandhinagar, Palaj, 382355, India
[3] Department of Geology and Geophysics, Indian Institute of Technology, Kharagpur, 721302, India
[4]Department of Geology Presidency University, Kolkata, 700003, India
[5]CSIR-National Geophysical Research Institute, Hyderabad 50000, India

Abstract

In this study, naturally occurring jarosite samples from Kachchh India (considered to be Martian analogue) were characterized using Fourier Transform Infrared Spectroscopy (FTIR), Cathodoluminescence- Energy Dispersive X-ray Spectroscopy (CL-EDXS) and luminescence (thermoluminescence (TL), blue and infrared stimulated luminescence (BSL and IRSL) methods. FTIR and CL-EDXS studies suggested that jarosite preserves its luminescence characteristics even after annealing the samples to 450°C. This facilitated luminescence studies (TL/BSL/IRSL) to assess the potential use of luminescence-dating methods to establish chronology of jarosite formation or its transport.

Jarosite exhibited TL, BSL and IRSL signals with varied sensitivities. The TL glow curve of jarosite comprises peaks at 100, 150, 300 and 350°C, reproducible under multiple readout cycles. The least bleachable peak at 350°C reduced to $(1/e)^{th}$ of its peak intensity (i.e. 36%) with ~100 minutes of exposure under a sun lamp. BSL and IRSL optical decay signals comprised three components. The signal exhibited athermal fading of g ~ 6 %/decade, but pIRIR signal at 225°C showed a near zero fading. The saturation doses ranged from 700 Gy to 2600 Gy for different signals, which suggest a dating range of 25 ka using a reported Martian total dose rate of 65 Gy/ka primarily due to cosmic rays. Multiple TL peaks and their widely differing stability also offer promise to discern changes in cosmic ray fluxes over century to millennia time scale through inverse modelling and laboratory experiments.

Keywords: Jarosite, Mars, Luminescence dating, Dose response, Thermoluminescence, Optically stimulated luminescence

1. Introduction

Considerable efforts are being made to understand the surface processes on Mars, largely through remote sensing methods (Howari et al. 2021; Lancaster and Greeley 1990; Rangarajan et al. 2018). Till date, the chronological information on surface processes is established through crater counting, which is a relative dating method that has a poor resolution and needs calibration (Doran et al. 2004). With the anticipation of sample return and onsite measurements by space missions, instruments are being developed and modelling/measurements of the properties of rocks on the Martian surface are being carried out (Jain et al. 2006; Lepper and McKeever 2000; Morthekai et al. 2007, 2008; Tsukamoto et al. 2011).

Luminescence techniques and in particular thermoluminescence (TL), has been used to understand the radiation, thermal history and the metamorphic grades of meteorites and lunar

samples (Biswas et al. 2011; Geake and Walker 1967; Sears et al. 2013). More recent efforts include the development of optically stimulated luminescence (OSL) readers for onsite dating and luminescence behaviour of minerals whose presence is reported in Martian sediments and rocks, such as pyroxene, olivine, gypsum, obsidian, anhydrite and various meteorites (Jain et al. 2006; Lepper and McKeever 2000; McKeever et al. 2003).

Luminescence dating is a widely used method for establishing chronologies of events associated with earth surface processes (Rhodes 2011; Singhvi et al. 2022). It utilizes radiation induced luminescence in natural minerals. A luminescence age is estimated by measuring the total luminescence and then scaling it with annual rate of luminescence production in a mineral. Appropriate laboratory calibration enables conversion of luminescence intensity to radiation dose units (energy deposited per unit mass) and is termed as paleodose. The annual rate of luminescence production (i.e. dose rate) is estimated by measuring the concentration of naturally occurring radioactivity viz. U, Th and K and the cosmic rays. In the case of Mars, the radiation dose is pre-eminently from cosmic rays (Morthekai et al. 2007) with a small contribution from the internal concentration of U, Th and K.

The use of luminescence signal for chronology requires that it remains stable over geological times and, this has to be ascertained for each sample/mineral phase/grain used for dating. Stability of a luminescence signal is determined by,

a) thermal kinetics, which depends on the ambient temperature, crystal properties and trap depth of trapping centres. Trapping of charges in these centres are assumed to follow the Arrhenius equation and
b) temperature independent, athermal quantum mechanical tunnelling effects, which results in reduction in trapped charges at a time dependent rate(Wintle 1973). Laboratory measurements along with modelling is used to correct for such a loss of signal through time (Huntley 2006; Kars et al. 2008).

Several minerals are used as luminescence chronometers. These include quartz, feldspar, gypsum, calcite, olivine, zircon, pyroxene, basalts and volcanic ashes (Aitken 1985; Biswas et al. 2013; Clark-Balzan et al. 2021; Jain et al. 2006; Nagar 2007; Zhang and Wang 2020). The abundance of quartz on Mars is negligible (Smith and Bandfield 2012). Much of the feldspar on the Martian surface is of basaltic origin, and should therefore be prone to athermal fading (Wintle 1973). Morthekai et al. (2008) demonstrated that athermal fading for the basalts cannot be adequately corrected. Further, presently available models do not ensure proper corrections (Biswas et al. 2013; Gliganic et al. 2012; Rajapara 2014), and to an extent, this limits the use of basaltic feldspars as a geochronometer on Mars.

Spectroscopic measurements from Mars missions viz., *Curiosity*, *Mars Pathfinder* and others, suggest the presence of jarosite on the surface of Mars. Morris et al. (2000) used optical and Mossbauer spectroscopic data from the Pathfinder mission to confirm the presence of jarosite. Rovers *Opportunity* (MER-B) and *Curiosity* (Klingelhöfer et al. 2004) reconfirmed the presence of jarosite using Mossbauer spectroscopy. Formation of jarosite requires wet (but water-limited) and acidic environment, and therefore its very presence implies the existence of water. Additionally, jarosite has the ability to incorporate foreign molecules in its structure e.g., glycine has been detected in natural jarosite on earth (Kotler et al. 2008). This adds value to the mineral in detecting biological activity on Mars.

Since, Jarosite is a widespread mineral on Mars surface, it can be used to study surface process on Mars and establish the associated timing of related processes. This work attempts

to characterize the luminescence dosimetry and dating properties of jarosite in order to explore its feasibility for dating Martian surfaces.

2. Formation and chemical properties

Jarosite is an anhydrous sulphate of the "alunite super group" with a general composition $AFe_3(SO_4)_2(OH, H_2O)$, where A is a metal (such as Ag, 1/2Pb, Na, K Rb Tl, 1/2Hg or hydronium). For jarosite, A is potassium. In nature, five kinds of metal substitutions can occur forming hydronium (hydronium jarosite), sodium (natrojarosite), silver (argentojarosite), lead (plumbojarosite) and ammonium (ammoniojarosite) (Roca 2022).

Jarosite forms through the weathering of sulphide ores in acidic sulphate soils or through oxidation of iron by microorganisms under bioleach environments (Roca 2022). It's occurrences are reported from USA, Brazil, Canada, Iran, Romania, Greece and India (Bhattacharya et al. 2016a; Klingelhöfer et al. 2004; Marescotti et al. 2010; Reynolds 2007; Velasco et al. 2013; Viñals et al. 1995, 2003). Jarosite occurs in four distinctive settings, viz. a) in sulphide ores due to oxidation or in arid areas with pyrite-bearing rocks; b) as nodules in clays; c) as segments of acid soils and; d) as hypogene minerals (Dutrizac and Jambor 2000). Synthetic jarosite can be prepared by heating the metal sulphate and sulphuric acid solution at ~100°C, leading to its precipitation (Dutrizac and Kaiman 1976; Fairchild 1933).

Jarosite structure comprises alternating tetrahedral and octahedral sheets. $Fe(O,OH)_6$ occupies octahedral sites connected by four hydroxyl groups, and with a neighbouring octahedral sheet and with two oxygen atom of $[SO_4]$ at a tetrahedral site (Xu et al. 2010). Metals (Ag, Pb, Na, K Rb Tl, Hg etc) reside in a 12-fold coordinated site, linked to 6 atoms of O from neighbouring $[SO_4]$ and 6 atoms from OH in $Fe(O,OH)_6$.

Numerous studies on the thermal stability of jarosite exist. Neutron diffraction studies on deuterated jarosite shows that jarosite is stable up to 277°C, beyond which it decomposes into yavapaiite, hematite and D_2O vapour (Xu et al. 2010). At 302 ° C, diffraction peaks of yavapaiite and hematite appear and jarosite gets decomposed at 327°C as follows,

$$KFe_3(SO_4)_2(OD)_6 \rightarrow KFe_3(SO_4)_2 + Fe_2O_3 + 3D_2O \quad (1)$$

Thermogravimetric and mass spectrometric analysis show successive mass loss from 130 - 330°C in K jarosite which has been attributed to the loss of water. The weight loss at 500°C, has been attributed to loss of sulphur, (Frost et al., 2005). For Na-jarosite, mass loss occurs between 215 - 230°C, followed by further mass losses at 352°C and 555°C. For Pb-jarosite mass loss occurs at 390°C and 418°C. Presence of Fe^{3+} in jarosite is responsible for its magnetic properties (Inami et al. 2000; Wills et al. 2000). It may be noted that jarosite decomposes in alkaline and acidic media; and it does not dissolve in water (Cruells and Roca 2022).

3. Samples and Methods

3.1. Sample details

Table 1 provides the details of six natrojarosite samples collected from Kachchh, India, for this study. The samples were from different stratigraphic units in sediment successions at Kachchh. The relevant part of the Mesozoic succession is described by Desai and Saklani (2012), and the Tertiary stratigraphy is documented in Biswas (1992). Samples 57D2 and 56B2 are from the Guneri member of the Mesozoic Bhuj Formation. Samples 65B2, 66B2

and 67F2 are from the Upper Palaeocene to Lower Eocene Naredi Formation, and sample 68B2 is from the Middle Eocene Harudi Formation. The host rocks are predominantly shales, with natrojarosite occurring in veins that cut across and are also parallel to the layering. Bhattacharya et al. (2016) established the presence of jarosite in the Matanumadh Formation of Kachchh using X-ray diffraction and FTIR methods, and the mode of occurrence was used by them to present the locality as a mineralogical Martian analogue. The present study includes jarosites from a location near to the Matanumadh Formation given in Table 1 and shown in Figure 1.

3.2. Measurement techniques

FTIR spectra of the powder samples were measured using a NICOLET 6700 (Thermo Fisher Scientific Instruments, USA) at the Central Research Facility at the Indian Institute of Technology Kharagpur. CL imaging was performed using Hitachi S-3400 N at the CSIR-National Geophysical Research Institute, Hyderabad with 15kV electron beam. The EDXS spectra was measured with electron beam focused on luminescing phases, using Oxford Ultim max 40 system and Aztec© software was used to obtain the EDXS spectra, having a total of 100% for each luminescence point.

TL and OSL were measured on fine grain (4-11 µm) fractions of Jarosite samples using a commercial Risoe TL/OSL reader DA-15 (with facilities for linear heating, blue (450-490 nm) or infrared (817-883 nm) LEDs for optical stimulation) at the Physical Research Laboratory, Ahmedabad. The detection optics comprised an EMI 9635 QA photomultiplier coupled to, a) a Schott BG-39 filter (330-625 nm) for TL; b) U340 (300- 380 nm) for BSL and pIRIR225 and c) Schott BG39+BG3 transmitting in 400-480 nm for IRSL(Bøtter-Jensen et al. 2003; Thomsen et al. 2006). A Sr^{90}/Y^{90} beta source, calibrated for fine grain quartz (4-11 µm grains), was used. The dose rate for quartz was 0.033 and 0.056 Gy/s. The corresponding absorbed dose for fine grain jarosite calculated using the stopping power was 0.038 and 0.066 Gy/s respectively. A calibrated alpha source, Am^{241} with a strength of 0.074 $\mu m^{-2} min^{-1}$ was used for alpha irradiations (Singhvi and Aitken 1978). A linear heating rate of 2°C/s up to 450°C was used for TL measurements.
Thick source alpha counting and sodium iodide- thallium activated scintillation counter were used to estimate the U, Th and K concentration in the sample.

3.3. Measurements

Samples were characterized using Cathodoluminescence- Energy Dispersive X-ray Spectroscopy and Fourier Transfer Infrared Spectroscopy (FTIR) and for their thermally and optically stimulated luminescence characteristics. Key issues examined are the effect of heating on luminescence and attendant properties to establish the use of jarosite for geochronometry.

3.3.1. Sample characterisation

These studies were carried out to characterize jarosite before and after annealing to 450°C. For FTIR, finely powdered samples were pressed into pellets after mixing them with dehydrated KBr powder in weight ratio of 1:300. FTIR spectra of the powder samples were collected in a transmittance mode in the spectral range of 4000–400 cm^{-1} at the spectral resolution of 4 cm^{-1} and both, the samples as received and their fractions annealed to 450°C were measured.

For CL-EDXS measurements, samples were placed on 15 × 4 mm stubs with a double-sided tape. The samples were carbon-coated using a Hitachi E-1010 Ion Sputter carbon coating unit

operating under a vacuum of 1 Pascal with a current of ~14 amperes. The samples were examined in the CL mode, and the X-ray spectrum was taken by focusing the electron beam on the luminescent phases. EDXS on luminous portions was measured, and atleast 10 luminescent points for each sample (natural and annealed) were probed. EDXS spectra yielded elemental data in weight percentages corresponding to each spot. To make calculations and visualization easier, the average weight % of elements across all measured spots in a sample was calculated for both natural and annealed samples. Comparative analysis was then carried out by plotting the elements against their average weight percentages for each set of samples to understand the differences between the natural and annealed conditions.

3.3.2. Luminescence measurements

The measurements were carried out in an oxygen free ultrapure nitrogen environment. Though the samples were collected as bulk rock, in daylight but once received, the entire laboratory processing analysis were carried out under subdued red light (>630nm). Pre-treatment of the grains with 1N HCl for 2 minutes increased the luminescence yield in comparison to the samples as received and therefore all samples were treated with HCl and the measurements were carried out on fine grains mounted on standard stainless steel discs. Samples 56B2, had the highest luminescence sensitivity (LS, luminescence per unit mass and per unit radiation dose (counts/(mg/Gy)) and was therefore used for most of the analysis for TL/OSL properties. The following studies were carried out.

(a) *TL and OSL characteristics:* The TL glow curves were recorded from room temperature to up to 450°C at a heating rate of 2°C/s. Measurements were done on natural samples (as received) and the same samples after an irradiation of 19 Gy to investigate the effect of heating above the decomposition temperature of jarosite on the glow curve. Blue stimulated luminescence (BSL) was recorded at 200°C for 100 sec after a preheat of 250°C for 10 sec and infrared stimulated luminescence (IRSL) was measured with sample at 50°C and 225°C for 100 sec and after a preheat of 250°C for 60 sec.

(b) *TL Sensitivity:* LS of 80-100°C peak was measured for all the samples by heating to 250°C then giving a dose of 19 Gy and normalizing the counts by the weight. The effect of heating on LS was compared by integrating the photon counts between 50-200°C by heating to 250°C and 450°C and normalizing them by weight. The protocol is given in Figure S1a.

(c) *Reproducibility:* The protocol in Figure S1b was used to measure the effect of repeated irradiation, heating cycle and measurement (TL/BSL/IRSL) to check the reproducibility of the signals.

(d) *Thermal stability:* Kinetic parameters such as activation energy E(eV)), frequency factor ($s(s^{-1})$), and the lifetime of charges in their trap (τ(s)) were estimated using fractional glow method (Gobrecht and Hofmann 1966; Pietkun et al. 1992; Shalgaonkar and Narlikar 1972). Three aliquots of the sample 56B2 were irradiated with 325 Gy beta dose, heated to 40°C (T_i), cooled to room temperature and then heated again to T_i+10°C. This was repeated till 450°C. The activation energy and lifetime for each cycle was estimated from the Arrhenius plot and by fitting the luminescence intensity with temperature using the equation.

$$I = -\frac{dn}{dt} = nse^{\frac{-E}{kT}} \qquad (2)$$

(e) *TL bleachability:* Bleachability of various TL glow peaks under exposure to solar simulator lamp (Osram, Ultravitalux, 300 watts filtered through a window glass) was investigated. Towards this, aliquots of sample 56B2 were annealed to 450°C, irradiated

(300 Gy) and bleached under solar lamp for time periods varying from 0 to 1000 minutes. The integrated photon counts (±5°C the peak counts) of glow peaks 150, 210, 300 and 350°C were weight normalized and plotted with bleach times.

(f) *Dose response curve:* The growth of luminescence signal (TL/BSL/IRSL) with radiation dose was studied. Single aliquot regenerative (SAR) type protocol was used to construct the dose response curves (DRC) (Murray and Wintle 2000). The DRC was fitted with following single saturating exponential equation

$$I = I_0(1 - e^{-\frac{D}{D_0}}) \quad (3)$$

where, I is the intensity at dose (D), and D_0 is the saturation dose defined as the dose where the intensity is 66% of maximum intensity (I_0). The maximum dose that can be estimated is till $2D_0$, after which the error increases.

The recycling ratio (ratio of luminescence produced by same dose but at different cycles of the protocol) and recuperation (ratio of luminescence due to zero dose to natural dose) were measured for a repeated and zero dose respectively. For TL, as the samples showed good reproducibility and therefore SAR with no sensitivity correction was used. For BSL and IRSL sensitivity correction used test dose normalisation. A modified version of protocols suggested by Wintle and Murray (2006) was used to construct the dose response curve for BSL 200_{UV}. Here the measurement was carried out at 200°C to prevent recapture of charges in glow peaks < 200°C.

For IRSL, measurements were made at 50°C in blue detection window (Wallinga et al. 2000), IRSL at elevated temperature of 225°C was also measured in UV and blue detection windows after measurement of IR50, as for pIRIR protocol for feldspars, (Buylaert et al. 2009). The measurement protocols are given in Table 2.

(g) *Athermal fading:* Athermal fading was estimated by irradiating the sample to a fixed (100 Gy) beta dose, followed by measurement after variable time delays The protocol is given in Figure 10 (Huntley 2006; Huntley and Lamothe 2001; Kars et al. 2008).

(h) Dose rate Estimation

a. *Alpha and Charge Particle Luminescence induction efficiency:* The track length of charge particles in a crystal matrix depends on their mass and energy. Thus dose deposition by alpha particles with higher mass and charge, results in a short track length along which higher ionization density imply loss of charges being trapped and consequence reduction in luminescence production / unit dose of alpha as compared to weakly ionizing beta particles (Aitken 1985; Zimmermans 1972). For low energy alpha particles, as in the case of terrestrial sediments, a ratio of luminescence produced per unit dose of alpha to beta called as alpha efficiency (a-value), is measured, and is included in computation of annual dose rate. The a-value is measured by bleaching the samples for 5 hrs and irradiating using ^{241}Am, in a vacuum alpha irradiator, (Singhvi and Aitken 1978) for 120 minutes. The protocols used to recover the dose are as per Table 2 were used to measure the "a-value".

b. On the Martian surface the major source of ionizing radiation is largely high energy protons and limited studies so far (Jain et al. 2007) suggest that the luminescence production efficiency would be in the range 0.5 to 1. Pending these measurements for the case of Jarosite, we used a luminescence production efficiency of 1 for integrated cosmic ray flux on Mars.

Measurements: Thick source alpha counting, where an alpha thick layer (~2mm) of sample is mounted on perplex holder being in direct contact with ZnS:Ag scintillator and

scintilations/unit area /unit time were measured to estimate U, Th concentration. NaI-scintillation counting was used to measure K concentration through the 1.46 MeV gamma ray from ^{40}K, the sample was mounted in plastic vials, with same geometry as the standard (AR grade KCl) and background and the concentration is estimated by peak area comparison method.

4. Results

FTIR and CL EDX studies were carried out to ascertain possible structural changes in Jarosite due to heating.

4.1.FTIR

The mid-infrared spectra of samples 57D2 and 57D2A and 66B2A were typical of jarosite, Figure 2 (Bhattacharya et al. 2016c; Bishop and Murad 2005; Cloutis et al. 2006; Farmer 1974; Sarkar et al. 2022). Spectra of 57D2 and 66B2 were nearly identical. The difference between the spectra of the annealed and non-annealed samples is that the non-annealed sample spectrum shows a higher overall absorbance, indicating larger proportion of crystalline jarosite. The spectral absorptions attributed to jarosite used in this study are listed in Table 3.

4.2.CL-EDXS studies

The comparison of EDXS spectra for natural and annealed samples (Figure 3) indicated that in most samples, annealing leads to a relative decrease in oxygen and aluminium, and an increase in potassium and sulphur concentrations. The iron content for sample 66B2, 57D2 remained unchanged, after annealing and decreased for 65B2 and 68B2. The calcium concentration in 65B2 and 68B2 on annealing increased from 6.6% to 25.5% and 1.6% to 8.2% respectively. These variations indicate that annealing did alter elemental distribution to a limited extent, suggesting changes in crystal structure or elemental diffusion and were sample dependent.

4.3.Luminescence measurements

4.3.1. TL glow curves

Figure 4 shows the weight normalized TL glow curves of natural and irradiated jarosites. Natural jarosite comprises a broad glow peak from 200°C to 450°C and the beta irradiated samples had additional glow peaks at 100, 150°C. Figure 6, shows the TL glow curve of sample 56b2 sample at 260 Gy, were 100 and 150°C peaks cannot be distinguished. This suggests that jarosite have multiple convoluted peaks, possibly at 100, 150, 300 and 350°C.

Figure S2a shows the results for multiple cycles of irradiation and heating to 250°C i.e. below the temperature for loss of stoichiometric water. Figure S2b shows the luminescence intensity with measurement cycles of repeated irradiation and readout. Figures S3a and S3b show changes in glow curve shape and luminescence sensitivity after cut heating to 450°C. In both cases and for all the glow peaks in multiple cycles of heating to 250°C and 450°C, the reproducibility of luminescence intensity was within 1 % and 6% respectively. This suggest that despite heating, the luminescing phase remains unaltered and these accord with FTIR and EDXS results.

Figure 5 shows that the LS between samples from different location is variable. Guneri jarosite has the highest LS. After heating to 450°C, LS for sample 66B2, 57D2, 56B2 decreased, while it increased for the samples 65B2, 67F2 and 68B2. Further, Figure 6, showed that heating to 450°C changes the LS of the sample; however, the glow curve shape does not change.

4.3.2 Stability: Kinetic Parameters:

Figure 7 provides the plot of activation energies with maximum temperature of heating for both unannealed and annealed samples. Regions of plateau are marked as a suggestion of a charge trap. The activation energy was same for annealed and non-annealed sample till 300 °C, after which deviation occur. Table 4 provides the data. Assuming a first order kinetics, the life time for glow peak centered at 350 °C glow peak in the case the unannealed sample is ~0.3Ma. For the annealed sample, two plateau above 300 °C are observed, with the highest lifetime of ~31Ma for glow peak at 360 °C peak. Further, there exist regions of continuous increase in the activation energy (from room temperature to 100 °C, from 240-300 °C) suggesting additional closely lying traps.

TL Dose Response Curve (DRC) and fading:

Since TL glow curves show reproducibility within a ~5-6%, single aliquot regenerative (SAR) protocol (Table 2), the luminescence vs. dose response curve (DRC) was constructed, without the use of conventional test dose sensitivity correction. Figure 8 shows the DRC of sample 56B2. The growth curve was fitted to a single saturating exponential, with equal weightage to all data points. TL glow peaks at 210 and 350°C have saturation doses ~ 2600 and 1600Gy respectively. The recycling ratio and recuperation were within 10 and 5% respectively, suggesting that the SAR protocol was suitable for estimating the absorbed doses using TL. Athermal fading with a g-value of 4.27%/decade and near zero was observed for the 210 and 350°C peaks. A-value for alpha particles was 0.075 and 0.051 for the 210 and 350°C peak respectively and as mentioned above for protons on Mars, a-value of 1 was assumed.

Bleaching of luminescence under a Solar Lamp

The bleachability of sample 56B2 is shown in Figure 9. In this, the photon counts of glow peaks 150, 210, 300 and 350°C were weight normalized. TL intensity reduces to 1/e (36%) of the maximum intensity after 16, 20, 70 and 105 minutes of solar lamp exposure for glow peaks at 150, 210, 300 and 350°C. This rate would be expectedly higher on Martian surface, due to higher concentration of UV penetrating to the surface (Haberle 2015; Solomon et al. 2005).

4.3.2. Optically stimulated Luminescence

4.3.2.1.Blue Stimulated Luminescence (BSL) - characteristics

A typical blue stimulated luminescence decay curve (measured at 200°C, after a preheat of 250°C in the ultraviolet detection window) is shown in Figure 11, for sample 56B2 irradiated to 350 Gy (natural signal bleached using blue LED for 100 sec at 200°C). The decay comprises three components (Figure S6) and relevant parameters are summarized in Table S1. Figure S7 shows the reproducibility of different components of the BSL optical decay curve on repeated irradiation (40 Gy) and blue light stimulation. Reproducibility of three components of BSL 200_{UV} was within 10%. The reproducibility experiments suggested a need of LS correction in constructing DRC (Figure 11).

The saturation dose for $BSL200_{UV}$ are 867 ± 85 Gy. This signal has athermal fading rate of 6.64 ± 0.82 %/decade and its alpha efficiency (a-value) is 0.093± 0.01.

4.3.2.2.Infrared Stimulated Luminescence (IRSL)- characteristics

The jarosite samples also showed infrared stimulated luminescence in blue (400-480 nm). The optical decay curves of IRSL at 50°C are shown in Figures 9 and S8. Figure S9 shows the reproducibility of the sample. For the IRSL measurements the average deviation between repeated signals was 3, 3, 14 % for the fast, medium and slow components, respectively.

Dose response curve and fading

The saturation dose for IRSL50 is 1180 ± 180 Gy and the athermal fading *g-value* was 7.4 ±0.7 %/decade. Recuperation and recycling were <10%. Further the saturation dose for pIRIR225 UV detection window is 817±95 Gy and for pIRIR225 blue detection window is 685±36 Gy. Near zero athermal fading is obtained for both the pIRIR225 signals. The 'a-values' are of 0.058 ± 0.005, 0.041±0.004 and 0.029 ± 0.002 for IR50 (blue), pIRIR225 (blue) and pIRIR225 (UV), respectively.

5. Dose rate

Table 6 provides the details of the measured radionuclide concentration. Radionuclide dose for the present samples based on the measured radioactivity for concentration is 1.62±0.6 mGy/year. Thin atmosphere of Mars implies higher cosmic ray dose contribution to dose rate compared to the Earth. Calculation done using GEANT4 simulation (Morthekai et al. 2007) yields a cosmic dose rate estimation of 63 mGy/year for the solar minimum condition. Summing this with the measured internal dose rate approximates an average total dose rate of ~65 mGy/year for Martian surface assuming a TL induction efficiency of 1.

6. Discussion

Jarosite is abundant on Mars and its use for dosimetry and dating can inform both on cosmic ray fluxes through time and on time scales of various surface processes on Mars. This study characterized 6 jarosite samples from an analog site in Kachchh, India. Jarosite exhibited TL/BSL/IRSL. TL glow peaks were at 100, 150, 300 and 350°C in the detection range of 325-700 nm (Figure 4, 6). The similarity of glow curve shape after heating and re-measurement of TL also suggests that heating of jarosite at ~277°C and at ~352°C did not interfere with its luminescing phases (Figure 6). However, a change in the sensitivity of the samples with heating, did occur (Figure 5). Samples that show enhancement in the sensitivity were accompanied by decrease in iron and increase in calcium and those that exhibited a decrease in the sensitivity, the iron content does not change (Figure 3 and 5(b)). As iron is a well-established quencher of luminescence properties, the increase in luminescence sensitivity with decreasing in iron content appears plausible (Nambi 1977). Further, as jarosite signatures are visible in the annealed FTIR spectra, it is reasonable to infer that complete breakdown of jarosite does not occur on cut heating up to 450°C.

Luminescence dating depends on the basic premise that the initial luminescence signal was zero or near zero. This could occur for two contexts, first the formation event, where the radiation induced luminescence is abinitio zero. The second is bleaching due to daylight exposure and burial thereafter. Laboratory studies on bleaching show that the glow peaks could be bleached 100 min (Figure 9). On Mars, higher UV flux due to thin atmosphere (5 to 38 g/cm^2; Haberle 2015; Solomon et al. 2005) would ensure an even more effective bleaching, given that UV has a higher cross-section for photo-bleaching (Spooner 1987). The least bleachable peak (350°C), attains residual after 105 minutes exposure of solar lamp (Figure 9). The upper limit of dating and dose estimates is constrained by the saturation of the luminescence intensity with radiation dose and the stability of the charges in the trap. Various signal of jarosite show variable saturation. The saturation doses were 800 Gy ($BSL200_{UV}$); 1180 Gy (IRSL50 blue detection), 1600 Gy TL450 (350) (Figure 8 and 11). pIRIR225 UV detection window exhibited saturation dose ~750 Gy and for pIRIR225 blue detection window was 590 Gy (Figure 11). All these signals can be used for dating and dosimetry.

From the thermal stability analysis, a similarity in annealed and non-annealed values suggest that the trap structure remains unaltered till 300°C, after which deviation occur. However, a notional lifetime of 0.3Ma for the non-annealed samples puts a constraint to dating only young events on the surface (Figure 7, table 2).

Various other dating parameters like athermal fading, alpha efficiency were measured. The athermal fading rate shows that the BSL200, IRSL50 and TL450 (210 peak) had g values of 7.6, 7.4, 4.3 %/decade respectively and these have to be corrected for dose estimates. Alternatively, pIRIR225 signals and TL450 (350 peak) signals with near zero athermal fading can be useful (Figure 8, 11, table 5).

The alpha efficiency of jarosite for a particular detection window (BG39, blue and UV) correlates with athermal fading g- value. Lower g-value corresponds to lower alpha efficiency as suggested by Singhvi (1981) and this needs to be explored further. Future studies on jarosite samples from other locations are now needed to establish working parameters (a- value/ charge particle induction efficiency for possible dating signals. These values can be assumed for estimating the dose and date without *in situ* measurement,(e.g. Schmidt et al. 2018).

7. Potentials for Luminescence studies using Jarosite

1. *Mars surface processes:* The high temperature (>300°C) traps in jarosite can be used for dating and the relevant age can be calculated by the following classic equation

$$\text{Age} = \frac{\text{Total dose accumulated}}{\text{Annual accumulation of dose}} \quad (4)$$

   Dividing the saturation dose by the annual dose rate gives a working dating range of ~25,000 years to understand time scales of aeolian processes, reported by the *Perseverance* rover on Mars.

2. *Mapping of cosmic ray flux on the surface of Mars and its variation with depth:* The lower temperature trap 210°C peak bleaches in 20 min and has a saturation dose of 2600 Gy value and the higher temperature peak at 350°C bleaches in 105 minutes with a saturation dose of 1600 Gy, this can with some ingenuity be used to estimate the current cosmic ray flux and the fluxes during the past. A rover containing a TL readout instrument can be used to first bleach the latent signal at the surface of interest and re-measure it after a designated time to obtain an absolute measurement of the absorbed cosmic ray flux by the surface. Samples at depth can give insights of the cosmic ray flux gradient. The aspect of long term changes in cosmic ray fluxes through inverse modelling will be developed elsewhere. Thus luminescence can provide very accurate spatial and temporal mapping of the flux, throughout the surface of Mars.

3. *Terrestrial studies for late quaternary climate change:* Jarosite formation is indicative of the start of aridity in the region, and thus a proxy for climate change. On Earth, various lakes have jarosite deposition (Long et al. 1992). Since this study shows the possibility of directly dating the jarosite formation age itself and not the minerals and organics found nearby, it can give added understanding of contemporary climates.

8. Summary and Conclusion

Following are the major findings of this study:

1. HCl increases the luminescence yield, possibly due to the removal of gleying.

2. In the detection window of 325-700 nm TL glow peaks of Jarosite are at 100, 150, 300 and 350°C.
3. Jarosite luminescence can be stimulated by both blue and infrared light and detection in both blue (400-480 nm) and UV (280-380 nm) are seen.
4. The luminescence signals are reproducible under repeated cycles of irradiation and read out. Reproducibility of TL was <6 % and that of BSL/IRSL (<14 %).
5. Luminescence sensitivity (LS) of the samples was variable. Samples from the Guneri formation had highest sensitivity. Heating up to 450 °C, changed the LS but the glow curve shapes remained the same. This is also supported by FTIR and CL-EDXS.
6. Fractional glow curve analysis suggests that kinetic parameters of glow peaks below 300°C are similar for both the annealed and non-annealed sample. For higher temperature glow peaks deviation occur. The glow peak at 300°C has an estimated lifetimes of ~ 0.3 Ma and this is suitable for dating.
7. Both BSL and IRSL comprise 3 components.
8. Saturation doses of various luminescence signal range from 590Gy to 1600 Gy. Any or all of these could be used for dating.
9. Jarosite shows large fading of the BSL and IRSL, i.e., around 6.64 and 7.4 %/decade. In TL for glow peak at 210°C, a fading of 4.3 %/decade is observed. However, no fading is observed for the pIRIR225 in blue and UV detection window and for TL glow peak at 350°C.
10. The average dose rate on the Martian surface is ~65 mGy/year, giving a dating range of ~25,000 years.

Thus, the study suggests that jarosite provides an array of luminescence signals that can be used for dating recent aeolian activity, mapping cosmic ray flux accumulation on Mars and terrestrial paleoclimatic studies. Further, since pIRIR225 does not show fading, jarosite can be used for *in situ* dosimetry on Mars.

Author Contributions:

SG and AKS conceived of this study. HM, SM and SG collected the samples and carried out FTIR analysis. AP, JKY, DSS and DK carried out the CL-EDXS measurements. MS carried out the luminescence measurement in consultation with AKS. NC supervised luminescence measurements. MS collated all the data and wrote the first draft with the help of AKS and all authors contributed to its multiple refinements. The authors agreed to the final version presented here.

Acknowledgement:

AKS thanks DST-SERB for a Year of Science Chair Professorship that facilitated this work. The work carried out at PRL is supported by the Department of Space, Government of India.

References

Aitken M. J. 1985. *Thermoluminescence Dating*, Academic Press

Bhattacharya S., Mitra S., Gupta S., Jain N., Chauhan P., and Parthasarathy G. 2016a. Journal of Geophysical Research : Planets. 402–431.

Bhattacharya S., Mitra S., Gupta S., Jain N., Chauhan P., and Parthasarathy G. 2016b. Journal

of Geophysical Research : Planets. 402–431.

Bhattacharya S., Mitra S., Gupta S., Jain N., Chauhan P., Parthasarathy G., and Ajai. 2016c. Jarosite occurrence in the Deccan Volcanic Province of Kachchh, western India: Spectroscopic studies on a Martian analog locality. *Journal of Geophysical Research: Planets* 121:402–431.

Bishop J. L., and Murad E. 2005. The visible and infrared spectral properties of jarosite and alunite. *American Mineralogist* 90:1100–1107.

Biswas S. K. 1992. Tertiary stratigraphy of Kutch. *Jour. Pal. Soc. India* 37:1–29.

Biswas R. H., Morthekai P., Gartia R. K., Chawla S., and Singhvi A. K. 2011. Thermoluminescence of the meteorite interior: A possible tool for the estimation of cosmic ray exposure ages. *Earth and Planetary Science Letters* 304:36–44. http://dx.doi.org/10.1016/j.epsl.2011.01.012.

Biswas R. H., Williams M. A. J., Raj R., Juyal N., and Singhvi A. K. 2013. Methodological studies on luminescence dating of volcanic ashes. *Quaternary Geochronology* 17:14–25. http://dx.doi.org/10.1016/j.quageo.2013.03.004.

Bøtter-Jensen L., McKeever S. W. S., and Wintle A. G. 2003. Optically Stimulated Luminescence Dosimetry. *Optically Stimulated Luminescence Dosimetry* 1–355.

Buylaert J. P., Murray A. S., Thomsen K. J., and Jain M. 2009. Testing the potential of an elevated temperature IRSL signal from K-feldspar. *Radiation Measurements* 44:560–565. http://dx.doi.org/10.1016/j.radmeas.2009.02.007.

Clark-Balzan L., May V. R., and Preusser F. 2021. Luminescence Characteristics of Intraplate-Derived Olivines. *Geochronometria* 48:73–94.

Cloutis E. A. et al. 2006. Detection and discrimination of sulfate minerals using reflectance spectroscopy. *Icarus* 184:121–157.

Cruells M., and Roca A. 2022. Jarosites: formation, structure, reactivity and environmental. *Metals* 12:802.

Desai B. G., and Saklani R. D. 2012. Significance of the trace fossil Balanoglossites Mägdefrau, 1932 from the Lower Cretaceous Guneri member (Bhuj formation) of the Guneri dome, Kachchh, India. *Swiss Journal of Palaeontology* 131:255–263.

Doran P. T. et al. 2004. Mars chronology: assessing techniques for quantifying surficial processes. *Earth-Science Reviews* 67:313–337. https://www.sciencedirect.com/science/article/pii/S001282520400039X.

Dutrizac J. E., and Kaiman S. 1976. Synthesis and properties of jarosite-type compounds. *The Canadian Mineralogist* 14:151–158.

Dutrizac J. E., and Jambor J. L. 2000. Jarosites and Their Application in Hydrometallurgy. *Reviews in Mineralogy and Geochemistry* 40:405–452. https://doi.org/10.2138/rmg.2000.40.8.

Fairchild J. G. 1933. Artificial jarosites—the separation of potassium from cesium. *American Mineralogist: Journal of Earth and Planetary Materials* 18:543–547.

Farmer V. C. 1974. The infrared spectra of minerals. *Mineralogical society monograph*

4:331–363.

Frost R. L., Weier M. L., and Martens W. 2005. Thermal decomposition of jarosites of potassium, sodium and lead. *Journal of thermal analysis and calorimetry* 82:115–118.

Geake J. E., and Walker G. 1967. Laboratory investigations of meteorite luminescence. *Proceedings of the Royal Society of London. Series A. Mathematical and Physical Sciences* 296:337–346.

Gliganic L. A., Roberts R. G., and Jacobs Z. 2012. Natural variations in the properties of TL and IRSL emissions from metamorphic and volcanic K-feldspars from East Africa: Assessing their reliability for dating. *Radiation Measurements* 47:659–664. https://www.sciencedirect.com/science/article/pii/S1350448712000649.

Gobrecht H., and Hofmann D. 1966. Spectroscopy of traps by fractional glow technique. *Journal of Physics and Chemistry of Solids* 27:509–522.

Haberle R. M. 2015. SOLAR SYSTEM/SUN, ATMOSPHERES, EVOLUTION OF ATMOSPHERES | Planetary Atmospheres: Mars. edited by North G. R., Pyle J., and Zhang F. B. T.-E. of A. S. (Second E. Oxford: Academic Press. pp. 168–177 https://www.sciencedirect.com/science/article/pii/B9780123822253003121.

Howari F. M., Sharma M., Xavier C. M., Nazzal Y., and AlAydaroos F. 2021. Chronological Analysis and Remote Sensing of Craters on the Surface of Mars . *Frontiers in Environmental Science* 9. https://www.frontiersin.org/articles/10.3389/fenvs.2021.605893.

Huntley D. J., and Lamothe M. 2001. Ubiquity of anomalous fading in K-feldspars and the measurement and correction for it in optical dating. *Canadian Journal of Earth Sciences* 38:1093–1106.

Huntley D. J. 2006. An explanation of the power-law decay of luminescence. *Journal of Physics Condensed Matter* 18:1359–1365.

Inami T., Nishiyama M., Maegawa S., and Oka Y. 2000. Magnetic structure of the kagomé lattice antiferromagnet potassium jarosite KFe 3 (OH) 6 (S O 4) 2. *Physical Review B* 61:12181.

Jain M., Andersen C. E., Bøtter-Jensen L., Murray A. S., Haack H., and Bridges J. C. 2006. Luminescence dating on Mars: OSL characteristics of Martian analogue materials and GCR dosimetry. *Radiation Measurements* 41:755–761.

Jain M., Andersen C. E., Hajdas W., Edmund J. M., and Bøtter-Jensen L. 2007. OSL response to proton irradiation in some natural dosemeters: Implications for martian sediment dating. *Nuclear Instruments and Methods in Physics Research, Section A: Accelerators, Spectrometers, Detectors and Associated Equipment* 580:652–655.

Kars R. H., Wallinga J., and Cohen K. M. 2008. A new approach towards anomalous fading correction for feldspar IRSL dating - tests on samples in field saturation. *Radiation Measurements* 43:786–790.

Klingelhöfer G. et al. 2004. Jarosite and hematite at Meridiani Planum from Opportunity's Mossbauer Spectrometer. *Science (New York, N.Y.)* 306:1740–1745.

Kotler J. M., Hinman N. W., Yan B., Stoner D. L., and Scott J. R. 2008. Glycine

identification in natural jarosites using laser desorption Fourier transform mass spectrometry: implications for the search for life on Mars. *Astrobiology* 8:253–266.

Lancaster N., and Greeley R. 1990. Sediment volume in the north polar sand seas of Mars. *Journal of Geophysical Research: Solid Earth* 95:10921–10927.

Lepper K., and McKeever S. W. S. 2000. Characterization of fundamental luminescence properties of the mars soil simulant JSC Mars-1 and their relevance to absolute dating of martian eolian sediments. *Icarus* 144:295–301.

Long D. T., Fegan N. E., McKee J. D., Lyons W. B., Hines M. E., and Macumber P. G. 1992. Formation of alunite, jarosite and hydrous iron oxides in a hypersaline system: Lake Tyrrell, Victoria, Australia. *Chemical Geology* 96:183–202.

Marescotti P., Carbone C., Comodi P., Frondini F., and Lucchetti G. 2010. Mineralogical and chemical evolution of ochreous precipitates from the Libiola Fe-Cu-sulphides mine eastern Liguria, Italy. *Acta Mineralogica-Petrographica. Abstract Series* 6:346. https://eurekamag.com/research/037/105/037105004.php.

McKeever S. W. S. et al. 2003. Concepts and approaches to in situ luminescence dating of martian sediments. *Radiation Measurements* 37:527–534. https://www.sciencedirect.com/science/article/pii/S1350448703000258.

Morris R. V et al. 2000. Mineralogy, composition, and alteration of Mars Pathfinder rocks and soils: Evidence from multispectral, elemental, and magnetic data on terrestrial analogue, SNC meteorite, and Pathfinder samples. *Journal of Geophysical Research: Planets* 105:1757–1817. https://doi.org/10.1029/1999JE001059.

Morthekai P., Jain M., Dartnell L., Murray A. S., Bøtter-Jensen L., and Desorgher L. 2007. Modelling of the dose-rate variations with depth in the Martian regolith using GEANT4. *Nuclear Instruments and Methods in Physics Research, Section A: Accelerators, Spectrometers, Detectors and Associated Equipment* 580:667–670.

Morthekai P., Jain M., Murray A. S., Thomsen K. J., and Bøtter-Jensen L. 2008. Fading characteristics of martian analogue materials and the applicability of a correction procedure. *Radiation Measurements* 43:672–678.

Murray A. S., and Wintle A. G. 2000. Application of the single-aliquot regenerative-dose protocol to the 375 °C quartz TL signal. *Radiation Measurements* 32:579–583.

Nagar Y. C. 2007. Methodological aspects of radiation dosimetry of natural radiation environment using luminescence techniques: New minerals and application.

Nambi K. S. V. 1977. *Thermoluminescence: Its understanding and applications*, Instituto de Energia Atomica.

Pietkun A., Polakiewicz L., and Oczkowski H. L. 1992. Measurement System for Fractional Glow Technique. *Acta Physica Polonica A* 81:687–691.

Rajapara H. M. 2014. Some Unresolved Problems of Mineral Luminescence Relevant to Radiation Dosimetry.

Rangarajan V. G., Bharti R., Mondal S. K., Pradhan C., and Dutta S. 2018. Remote Sensing for Martian Studies: Inferences from Syrtis Major. *Journal of the Indian Society of Remote Sensing* 46:1537–1551. https://doi.org/10.1007/s12524-018-0826-7.

Reynolds G. A. 2007. the Jarosite Group of Compounds – Stability , Decomposition and Conversion.

Rhodes E. J. 2011. Optically Stimulated Luminescence Dating of Sediments over the Past 200,000 Years. *Annual Review of Earth and Planetary Sciences* 39:461–488. https://api.semanticscholar.org/CorpusID:64684744.

Roca A. 2022. Jarosites: Formation, Structure, Reactivity and Environmental.

Sarkar S., Moitra H., Bhattacharya S., Dagar A., Ray D., Gupta S., Chavan A., Shukla A. D., and Bhandari S. 2022. Spectroscopic studies on the Puga Hot Spring Deposits, Ladakh, an astrobiological Martian analog site in India. *Journal of Geophysical Research: Planets* 127:e2022JE007299.

Schmidt C., Bösken J., and Kolb T. 2018. Is there a common alpha-efficiency in polymineral samples measured by various infrared stimulated luminescence protocols? *Geochronometria* 45:160–172.

Sears D. W. G., Ninagawa K., and Singhvi A. K. 2013. Luminescence studies of extraterrestrial materials: Insights into their recent radiation and thermal histories and into their metamorphic history. *Chemie der Erde* 73:1–37. http://dx.doi.org/10.1016/j.chemer.2012.12.001.

Shalgaonkar C. S., and Narlikar A. V. 1972. Review: a review of the recent methods for determining trap depth from glow curves. *Journal of Materials Science* 7:1465–1471. https://doi.org/10.1007/BF00574938.

Singhvi A. K., and Aitken M. J. 1978. Americium-241 for alpha-irradiations. *Ancient TL* 2:2–9.

Singhvi A. K. 1981. A possible correlation between the alpha efficiency and the anomalous fading characteristics. *Ancient TL* 14:10.

Singhvi A., Kaushal R., and Parida S. 2022. Luminescence dating and Quaternary Geology: The Indian Narrative. *Journal of the Palaeontological Society of India* 67(1):183–210.

Smith M. R., and Bandfield J. L. 2012. Geology of quartz and hydrated silica-bearing deposits near Antoniadi Crater, Mars. *Journal of Geophysical Research: Planets* 117.

Solomon S. C. et al. 2005. New Perspectives on Ancient Mars. *Science* 307:1214–1220. http://www.jstor.org/stable/3840200.

Spooner N. A. 1987. The effect of light on the thermoluminescence of quartz.

Thomsen K. J., Bøtter-Jensen L., Denby P. M., Moska P., and Murray A. S. 2006. Developments in luminescence measurement techniques. *Radiation Measurements* 41:768–773.

Tsukamoto S., Duller G. A. T., Wintle A. G., and Muhs D. 2011. Assessing the potential for luminescence dating of basalts. *Quaternary Geochronology* 6:61–70. http://dx.doi.org/10.1016/j.quageo.2010.04.002.

Velasco F., Herrero J. M., Suárez S., Yusta I., Alvaro A., and Tornos F. 2013. Supergene features and evolution of gossans capping massive sulphide deposits in the Iberian Pyrite Belt. *Ore Geology Reviews* 53:181–203. https://www.sciencedirect.com/science/article/pii/S016913681300019X.

Viñals J., Roca A., Cruells M., and Núñez C. 1995. Characterization and cyanidation of Rio Tinto gossan ores. *Canadian Metallurgical Quarterly* 34:115–122. https://www.sciencedirect.com/science/article/pii/000844339400022C.

Viñals J., Roca A., and Arranz M. 2003. Autoclave Alkaline Decomposition and Cyanidation of Jarosite-Beudantite Phases from Rio Tinto Gossan Ores. *Canadian Metallurgical Quarterly* 42:29–40. https://doi.org/10.1179/cmq.2003.42.1.29.

Wallinga J., Murray A., and Wintle A. 2000. The single-aliquot regenerative-dose (SAR) protocol applied to coarse-grain feldspar. *Radiation Measurements* 32:529–533.

Wills A. S., Harrison A., Ritter C., and Smith R. I. 2000. Magnetic properties of pure and diamagnetically doped jarosites: model kagomé antiferromagnets with variable coverage of the magnetic lattice. *Physical Review B* 61:6156.

Wintle A. G. 1973. Anomalous fading of thermo-luminescence in mineral samples. *Nature* 245:143–144.

Wintle A. G., and Murray A. S. 2006. A review of quartz optically stimulated luminescence characteristics and their relevance in single-aliquot regeneration dating protocols. *Radiation Measurements* 41:369–391.

Xu H., Zhao Æ. Y., Vogel Æ. S. C., Hickmott D. D., Daemen Æ. L. L., and Hartl M. A. 2010. Thermal expansion and decomposition of jarosite : a high-temperature neutron diffraction study. 73–82.

Zhang J., and Wang L. 2020. Thermoluminescence dating of calcite – Alpha effectiveness and measurement protocols. *Journal of Luminescence* 223:117205. https://doi.org/10.1016/j.jlumin.2020.117205.

Zimmermans D. W. 1972. Relative thermoluminescence effects of alpha- and beta- radiation. *Radiation Effects* 14:81–92.

Luminescence Characteristics of Terrestrial Jarosite from Kachchh, India: A Martian Analogue

Malika Singhal[1,2], Himela Moitra[3], Souvik Mitra[4], Aurovinda Panda[5], Jayant Kumar Yadav[5], D. Srinivasa Sarma[5], Devender Kumar[5], Naveen Chauhan[1], Saibal Gupta[3], Ashok Kumar Singhvi[1]

[1]Atomic and Molecular Physics Division, Physical Research Laboratory, Ahmedabad, 380009, India
[2] Indian Institute of Technology, Gandhinagar, Palaj, 382355, India
[3] Department of Geology and Geophysics, Indian Institute of Technology, Kharagpur, 721302, India
[4]Department of Geology Presidency University, Kolkata, 700003, India
[5]CSIR-National Geophysical Research Institute, Hyderabad 500007, india

Tables

Table 1: Sample details

Sr. No.	Samples	Formation	Latitude	Longitude	Main lithology
1	56B2	Guneri	23º47´07´´N	68º50´22´´E	Shale, Sandstone, Laterite
2	57D2	Guneri	23º47´01´´N	68º50´22´´E	Shale, Sandstone, Laterite
3	65B2	Naredi	23º34´47´´N	68º38´52´´E	Shale, Limestone
4	66B2	Naredi	23º34´43´´N	68º38´38´´E	Shale, Limestone
5	67F2	Naredi	23º34´31´´N	68º38´36´´E	Shale, Limestone
6	68B2	Harudi	23º31´28´´N	68º41´08´´E	Shale, Limestone

Table 2: Various protocol used to estimate the dose.

Step. No.	TL450	$BLSL200_{UV}$ (modified after Wintle and Murray, (2006))	$IR50_{blue}$ (Wallinga et al. 2000)	$pIRIR225_{blue}$ (Buylaert et al. 2009)	$pIRIR225_{UV}$ (Buylaert et al. 2009)
1	Natural dose/ Regenerative dose	Natural dose/ Regenerative dose	Natural/ Regenerative dose	Natural/ Regenerative dose	Natural dose/ Regenerative dose
2	TL 250°C	Preheat 250 °C for 10 s	Preheat 250 °C for 60 s	Preheat 250 °C, 60 s	Preheat 250 °C, 60 s
3	TL 450°C	BSL at 200°C for 100 s	IRSL at 50°C for 100 s	IRSL at 50°C, 100 s	IRSL at 50°C, 100 s
4	Go to step 1	Test dose	Test dose	IRSL at 225°C, 200 s	IRSL at 225°C, 200 s
5		Preheat 250 °C for 10 s	Preheat 250 °C for 60 s	Test dose	Test dose
6		BSL at 200°C for 100 s	IRSL at 50°C for 100 s	Preheat 250 °C, 60 s	Preheat 250 °C, 60 s
7		Go to step 1	Go to step 1	IRSL at 50°C, 100 s	IRSL at 50°C, 100 s
8				IRSL at 225°C, 200 s	IRSL at 225°C, 200 s
9				Go to step 1	Go to step 1
Emission under investigation (nm)	330-625	280-380	400-480	400-480	280-380

Table 3: FTIR spectral absorption attributes of jarosite.

Wavenumber	**Molecular transition**	**Attribute**
449	ν2 (SO_4)-2	fundamental bending vibrations in sulphate ion
474	M-O(M:Al/Fe)	metal-oxygen vibrations
508	M-O(M:Al/Fe)	metal-oxygen vibrations
629	ν4 (SO_4)-2	fundamental stretching vibrations in sulphate ion
673	ν4 (SO_4)-2	fundamental stretching vibrations in sulphate ion
1012	δ(OH)	in-plane bending vibrations of hydroxyl ion
1025	δ(OH)	in-plane bending vibrations of hydroxyl ion
1094	ν3 (SO_4)-2	fundamental stretching vibrations in sulphate ion
1189	ν3 (SO_4)-2	fundamental stretching vibrations in sulphate ion
3358	ν (OH	fundamental stretching vibrations in hydroxyl ion

Table 4: Kinetic parameters for 56B2.

Peak	Sample as received followed by 325 Gy beta dose				Peak	Samples after heating to 450°C for 10 s followed by 325 Gy beta dose			
	Peak Temperature (°C)	Activation energy E (eV)	Frequency factor s (s^{-1})	Lifetime (s) at 27°C		Peak Temperature (°C)	Activation energy E (eV)	Frequency factor s (s^{-1})	Lifetime (s) at 27°C
A	150	0.82±0.04	(2±1) $\times 10^{9}$	(5.4±3.5) $\times 10^{4}$	A	150	0.83±0.04	(2.15±0.3) $\times 10^{9}$	(125±24) $\times 10^{4}$
B	210	0.94±0.04	(8.5±5.3) $\times 10^{8}$	(1.1±0.3) $\times 10^{7}$	B	210	0.93±0.04	(1.1±.1) $\times 10^{9}$	(3.5±3) $\times 10^{7}$
C	300	1.32±0.03	(9.4±10) $\times 10^{9}$	(4.8±3.6) $\times 10^{12}$	D	300	1.47±0.04	(2.75±2.25) $\times 10^{11}$	(13±13) $\times 10^{12}$
					E	360	1.63±0.04	(7.2±1.3) $\times 10^{11}$	(5±7) $\times 10^{15}$

Table 5: Dose response parameters.

Sr. No.	Protocol name	No. of disc	Saturation dose ($2D_0$)(Gy)	g-value (%/decade) (average of 10 aliquots)	Alpha efficiency	Recycling ratio (%)	Recuperation (%)
1	TL450 (210 peak)	2	2570±500	4.3 ±1	0.075±0.004	< 10	< 2
2	TL450 (350 peak)	2	1590 ±122	-1 ±0.7	0.051±0.004	< 10	< 1
3	$BSL200_{UV}$	3	867±85	7.6 ±0.6	0.093±0.01	< 10	< 2
4	$IR50_{Blue}$	3	1180± 181	7.4± 0.7	0.058±0.005	< 10	< 2
5	$pIRIR225_{UV}$	3	817±95	0.7±0.2	0.029±0.002	< 10	< 2
6	$pIRIR225_{blue}$	3	685±36	-0.5±0.4	0.041±0.004	< 10	< 2

Table 6: Summary of dose rate; Sample 67F2

Internal Dose rate (mGy/yr)	Concentration of radionuclide		Dose rate estimation technique
	U238 (ppm)	1.87± 0.1	ZnS alpha counting
	Th232 (ppm)	1.06 ±0.35	ZnS alpha counting
	K (%)	0.78± 0.07	NaI Scintillator, gamma counting
	Total internal dose rate	1.62±0.6 (mGy/yr)	
External dose rate (mGy/yr)	Cosmic Ray	63	Simulation; (Morthekai et al. 2007)
Total dose rate (mGy/yr)		65	

Figures

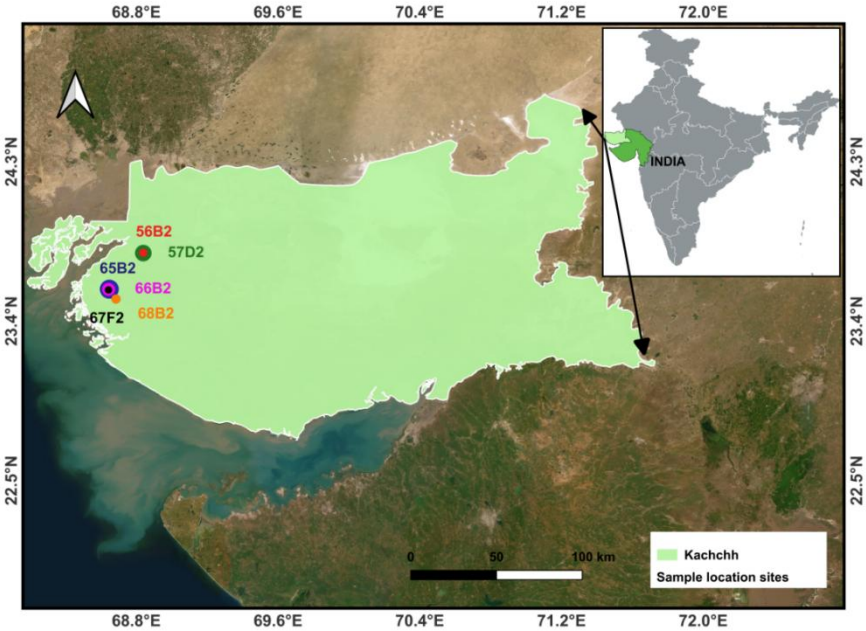

Figure 1: Map showing the location of samples used in this study.

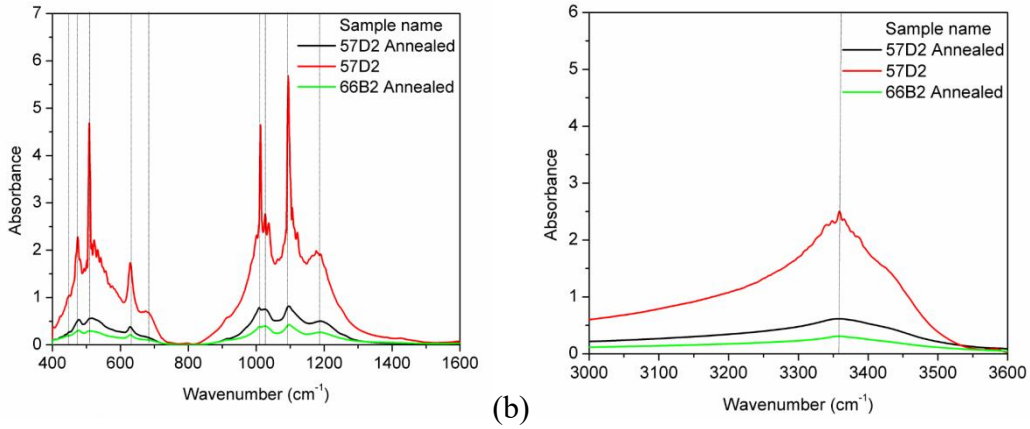

Figure 2: Mid-infrared spectra of samples 57D2, 57D2 Annealed and 66B2 Annealed from (a) 400-1600 cm^{-1} to study the fundamental absorptions and (b) from 3000-3600 cm^{-1} to study the absorptions due to the hydroxyl ion. These show that jarosite signatures are preserved even after annealing to 450°C. The marked lines are discussed in Table 3.

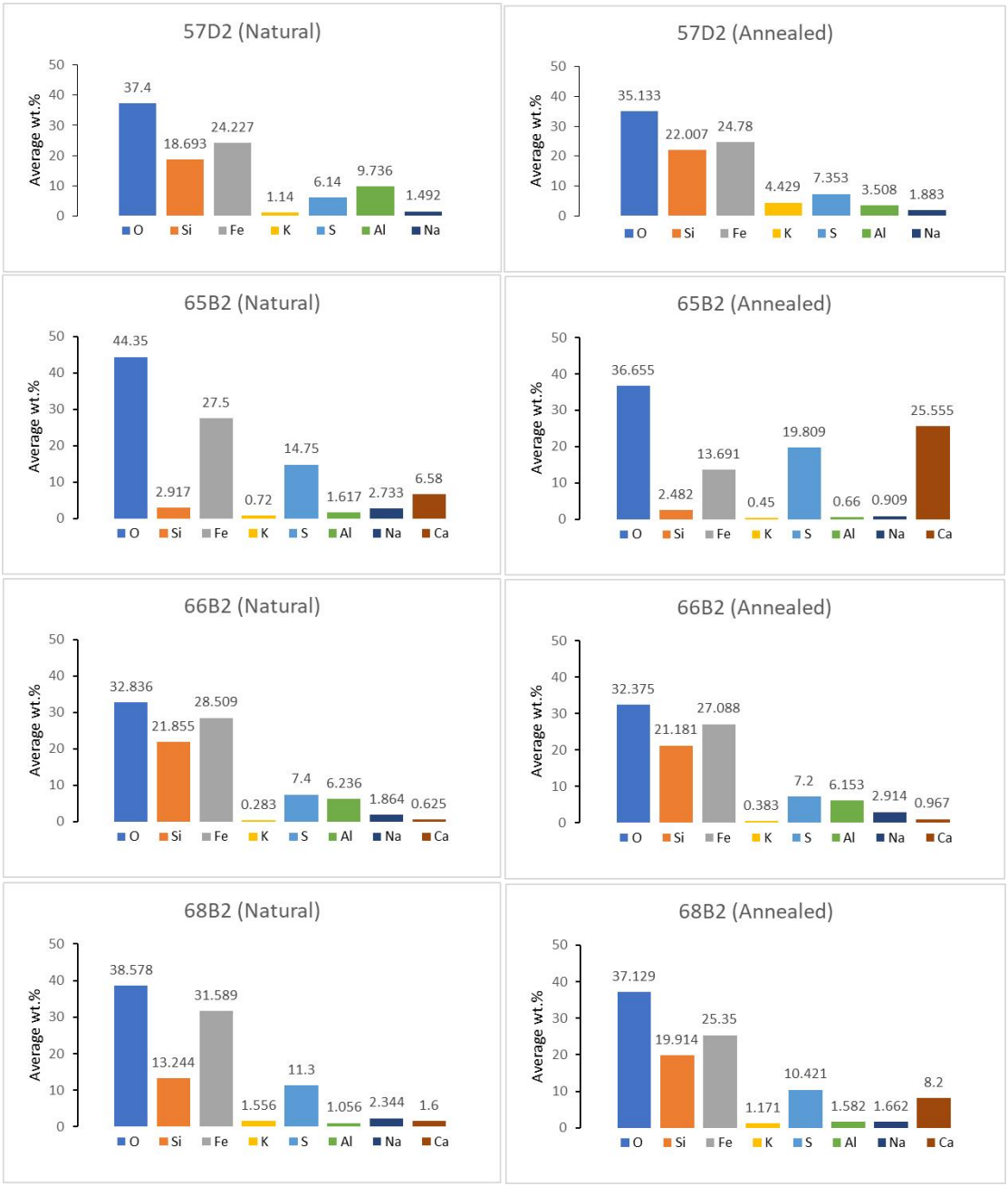

Figure 3: Elemental composition of phases luminescing under CL. natural and annealed samples. Annealing was at 450°C.

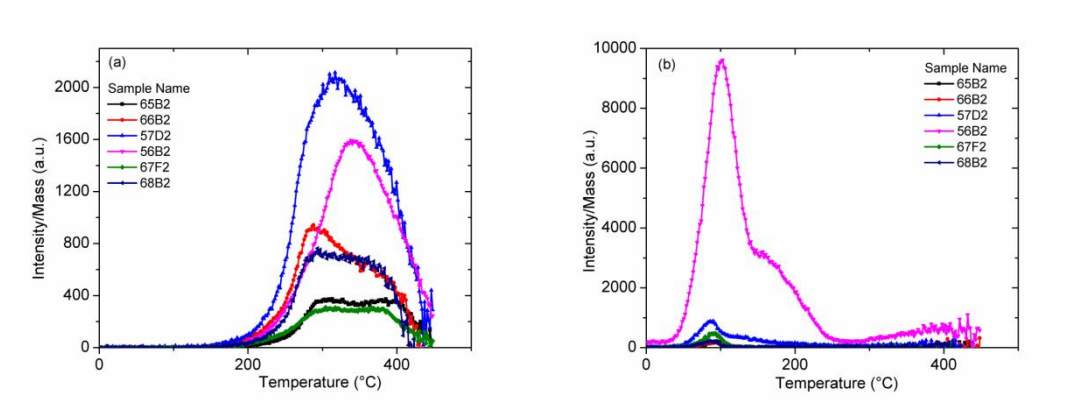

Figure 4. TL Glow Curves of samples in emission range 325-700 nm; a) Natural grains with HCl wash. (b) beta irradiated (19Gy) grain after a preheat of 450°C and given a dose of 19 Gy.

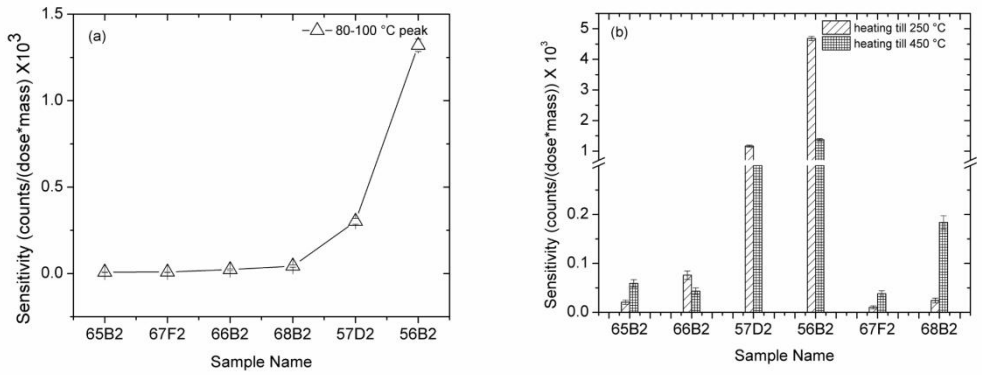

Figure 5: (a) Sensitivity of 80-100°C peak was measured for all sample by heating to 250°C then giving a dose of 19Gy. (b) Effect of heating to 250°C and 450°C on the sensitivity of 50-200°C peak.

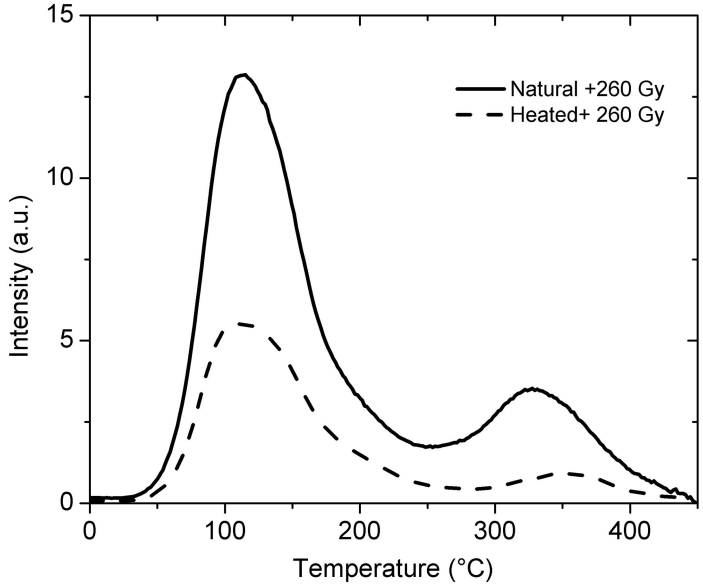

Figure 6: Sample 56B2. TL when the natural sample is given a dose of 260 Gy and when the same heated sample is given a dose of 260 Gy.

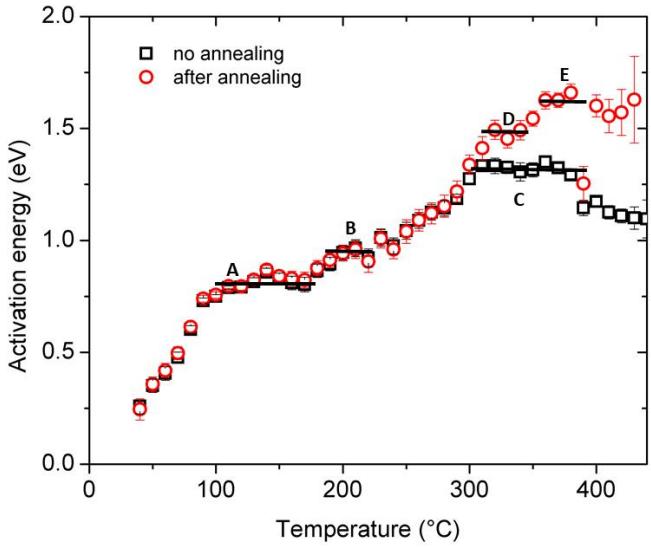

Figure 7: Activation energy versus maximum heating temperature graph for 56B2 obtained by Fractional glow curve method. Observation in emission range 325-700 nm.

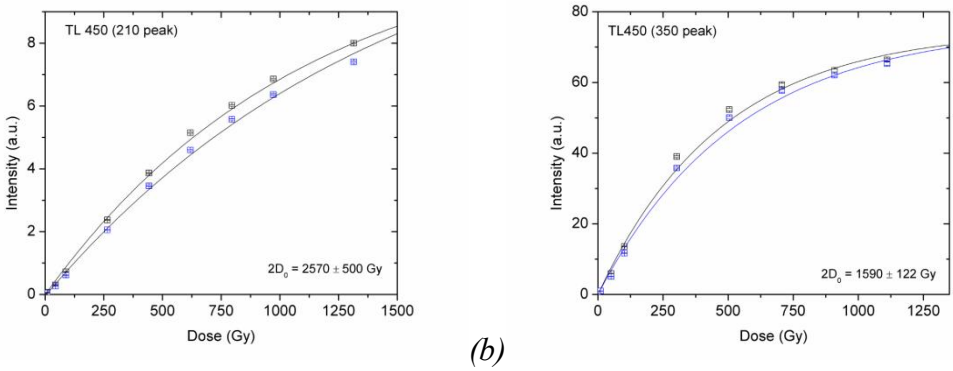

(a) *(b)*

Figure 8: Sample 56B2 TL dose response curve DRC. TL intensity comprises, (a) Integrated photon count 340- 360°C. (b) Integrated photon counts are from 200-220°C. Individual lines show data on from different aliquot.

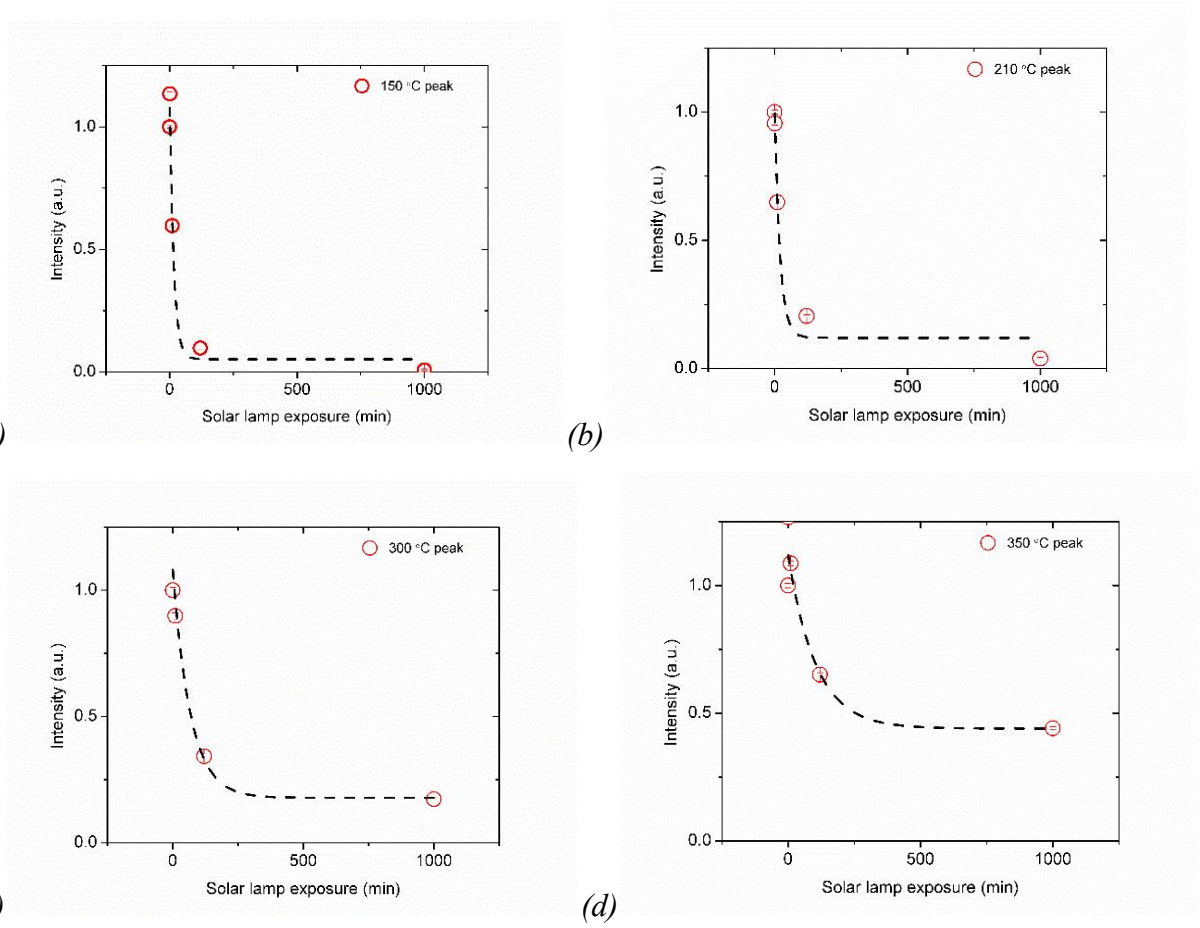

Figure 9: Solar lamp resetting of annealed sample 56B2 after a dose of 300 Gy for different TL peaks. Each data point is an average of three aliquots. The curves were fitted with $y=a.e^{-b.t.}$

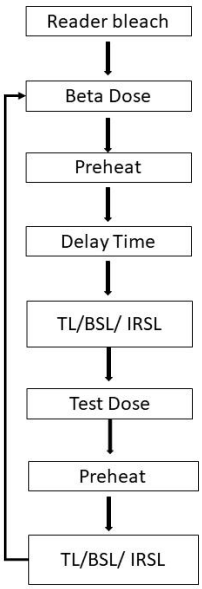

Figure 10: Protocol used to estimate fading.

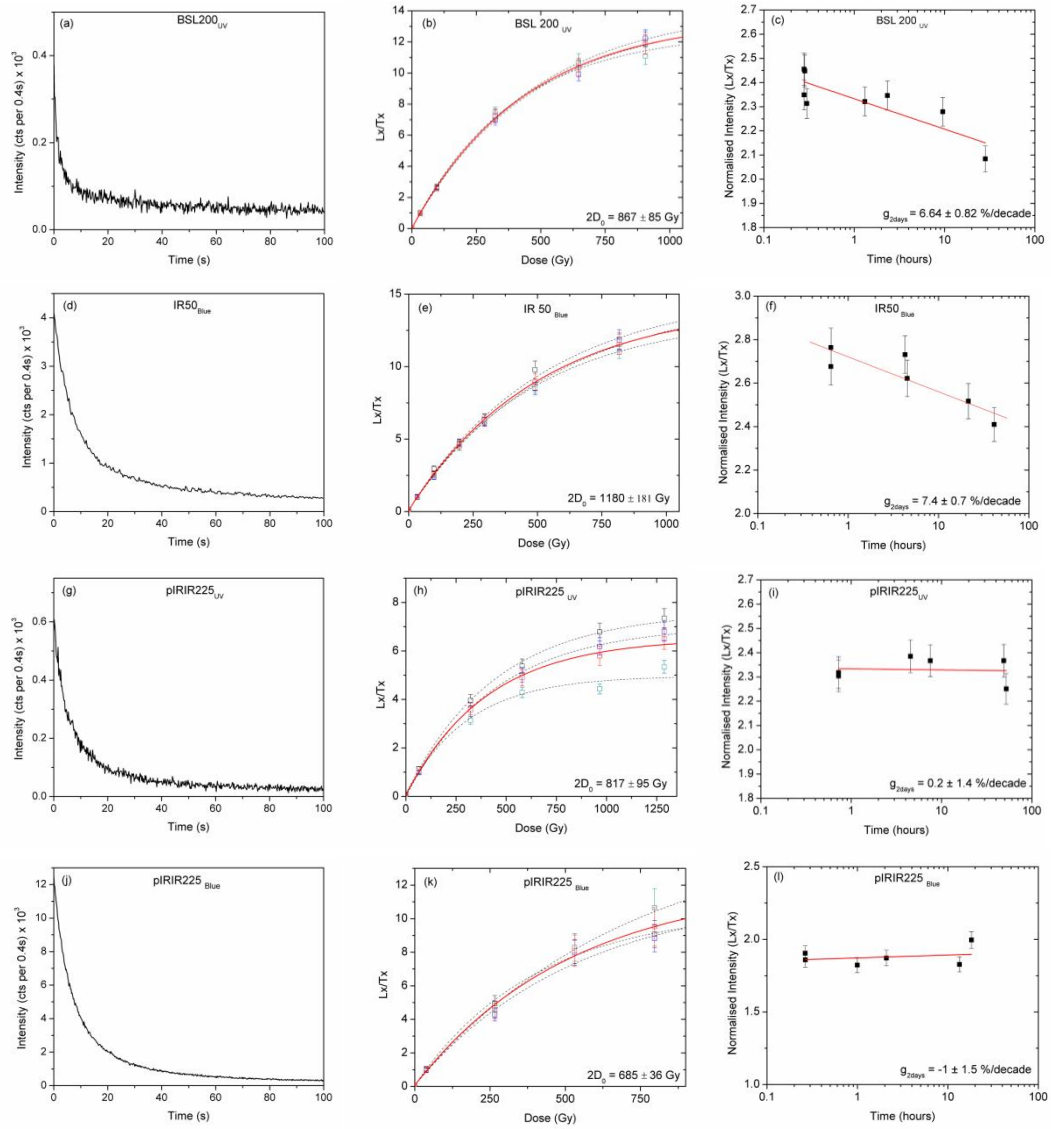

Figure 11: Optical decay curves (left); Dose response curves (middle), each dashed line is data on individual aliquot and solid line is average; Fading characteristics (right) of $BSL200_{Uv}$, $IR50_{Blue}$, $pIRIR225_{UV}$, $pIRIR225_{Blue}$ respectively.

Luminescence Characteristics of Terrestrial Jarosite from Kachchh, India: A Martian Analogue

Malika Singhal[1,2], Himela Moitra[3], Souvik Mitra[4], Aurovinda Panda[5], Jayant Kumar Yadav[5], D. Srinivasa Sarma[5], Devender Kumar[5], Naveen Chauhan[1], Saibal Gupta[3], Ashok Kumar Singhvi[1]

[1]Atomic and Molecular Physics Division, Physical Research Laboratory, Ahmedabad, 380009, India
[2] Indian Institute of Technology, Gandhinagar, Palaj, 382355, India
[3] Department of Geology and Geophysics, Indian Institute of Technology, Kharagpur, 721302, India
[4]Department of Geology Presidency University, Kolkata, 700003, India
[5]CSIR-National Geophysical Research Institute, Hyderabad 500007l,India

Supplementary File

Tables

Table S1: CW-OSL components of 56B2. The optical decay curves were deconvoluted using fit_cWCurve by (Kreutzer et al. 2024) using the equation $I = \sum_i I_i \sigma_i e^{-\sigma_i t}$ where, I_i is the initial concentration of charges of the ith component, σ_i is the decay constant, t is the time and photoionization cross-section (cs) calculated from the I_i, σ_i and the power, wavelength of the light stimulation used.

Signal	Components	Intensity (I_0) (arb. units)	Decay constant (σ) (s^{-1})	Photoionisation cross-section (cs) (cm^2)	R-squared
BSL at 25°C	c1 (slow)	3074±804	0.93±0.15	9.87E-18	0.9972
	c2 (medium)	10570±654	0.19±0.03	1.97E-18	
	c3 (fast)	56527±1519	0.01±0.001	1.49E-19	
IRSL 50°C	c1 (slow)	17538±6082	0.25±0.03	1.94E-19	0.9996
	c2 (medium)	62382±3129	0.09±0.01	6.99E-20	
	c3 (fast)	105514±1952	0.012±0.002	9.32E-21	

Figures

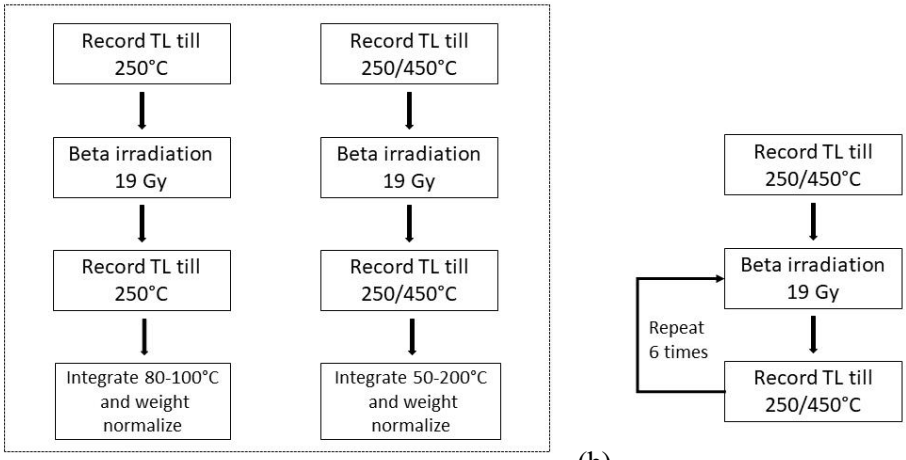

(a) (b)

Figure S1: Protocol for reproducibility measurement. Measurement condition were, heating rate 2°C and the luminescence detection was in 325-700 nm.

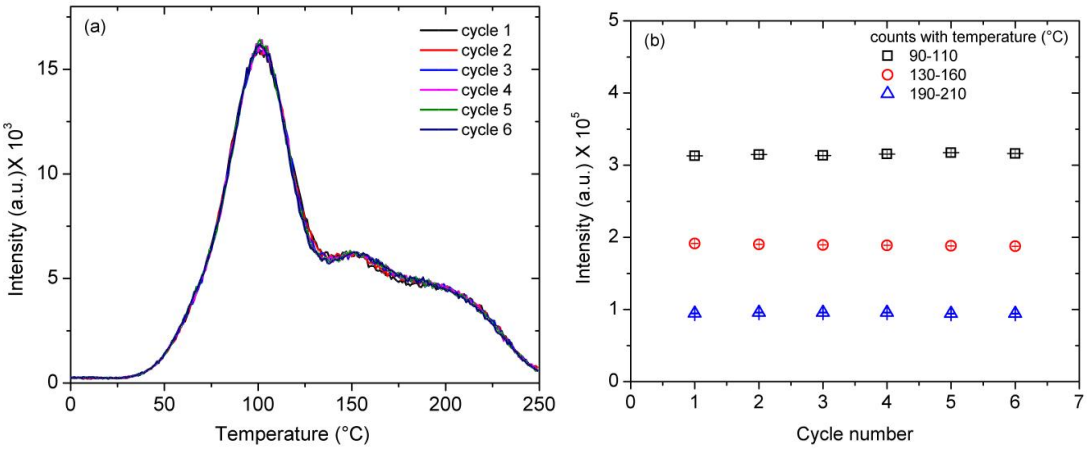

Figure S2: Sample 56B2. (a) Reproducibility of TL glow curve up to 250°C. (b) Photon counts integrated for repeated measurement cycles.

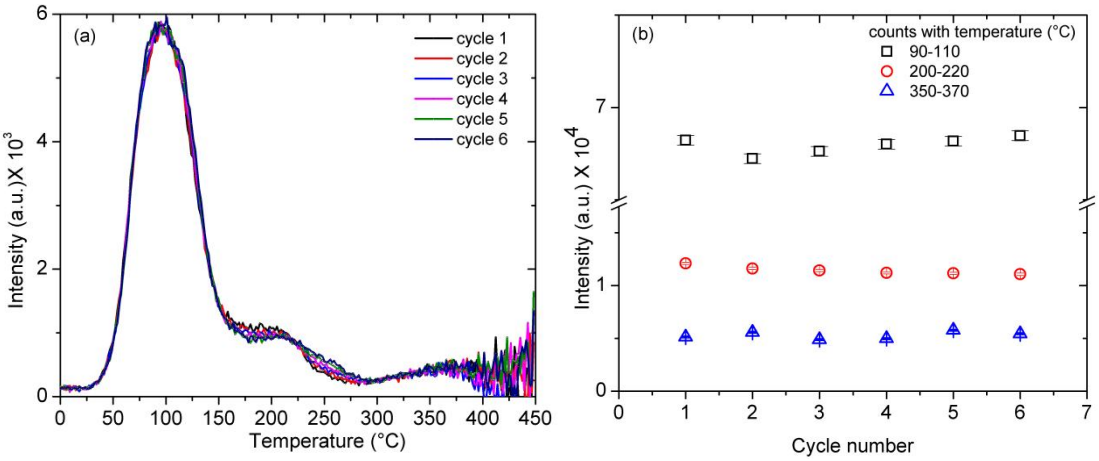

Figure S3: Sample 56B2. (a) Reproducibility of TL glow curves up to 450°C. (b) Photon counts integrated for repeated measurement cycles.

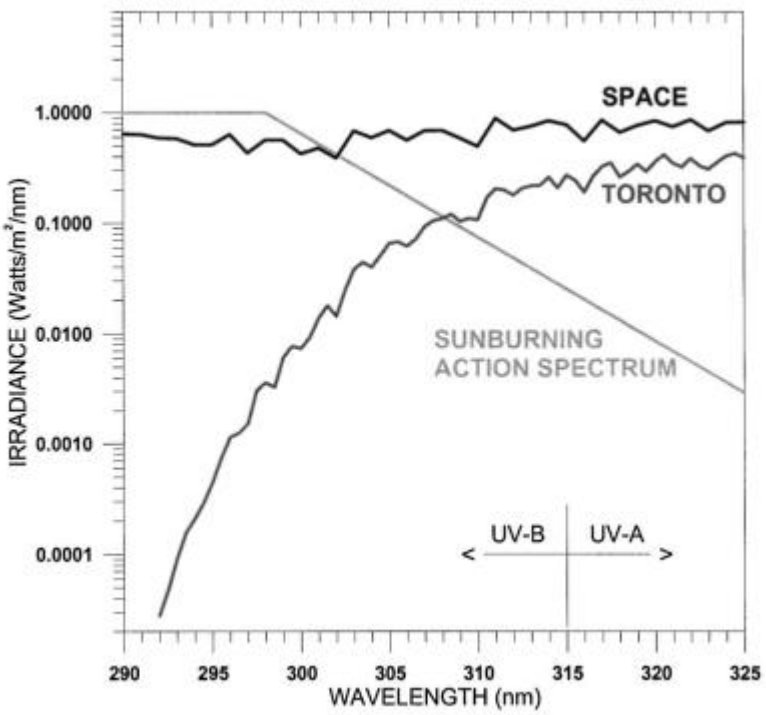

Figure S4: Space- and ground-based (Earth) spectral measurements of UV radiation. Absorption by atmospheric ozone causes the sharp cutoff of the ground-based spectrum of global irradiance around 290 nm. Figure taken from Kerr (2005)

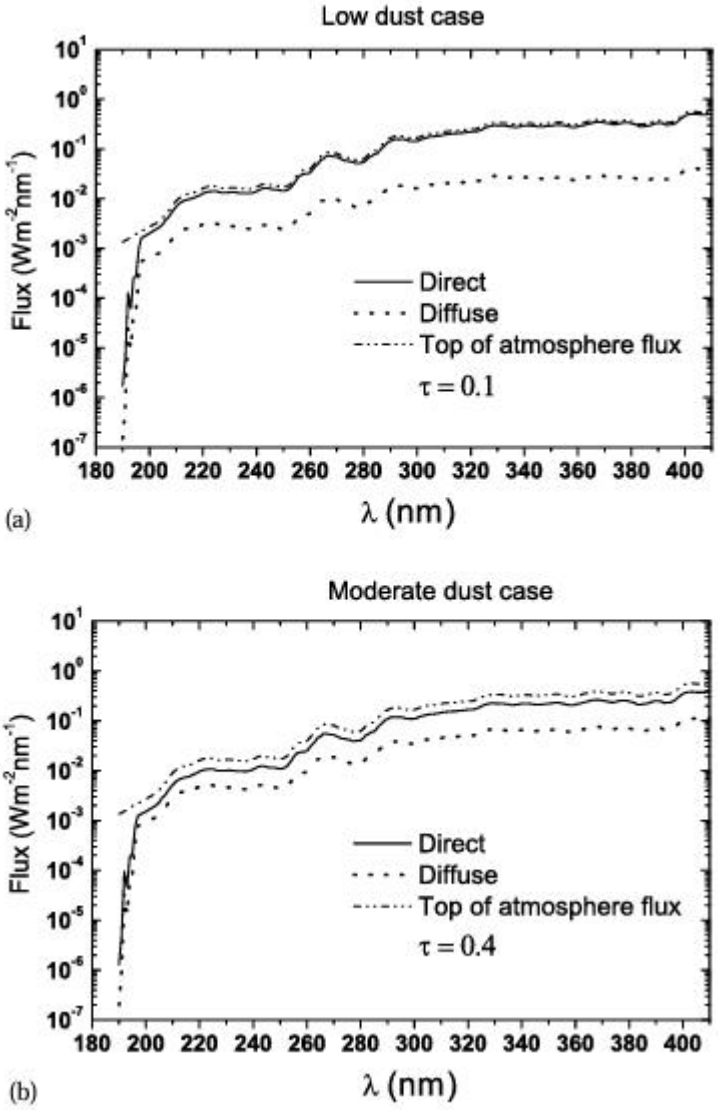

Figure S5: UV solar spectra penetrating the Mars atmosphere. Two cases during northern summer are shown here for the low dust case, at Ls =70◦, latitude = 0◦, local noon: (a) shows the case of the lower dust limit, τ =0.1. There is little modification of the input flux, except for the characteristic cutoff near 190 nm; (b) shows the upper limit for this period, with τ =0.4. There is still little change to the flux, but in comparison to (a) there is a greater difference between direct and diffuse fluxes. Figure taken from Patel et al. (2002).

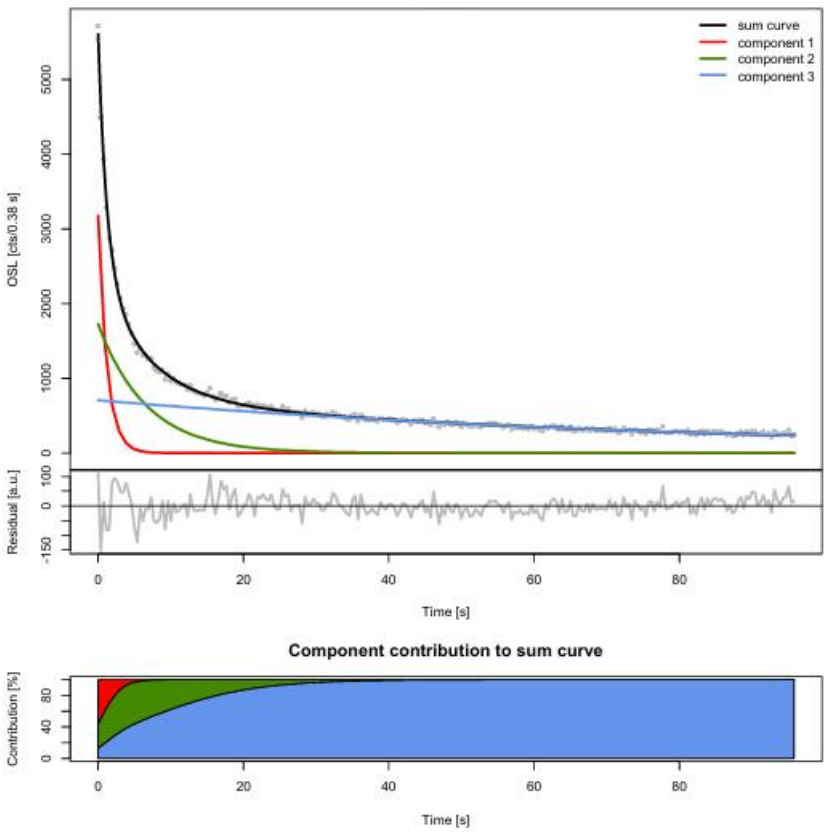

Figure S6: Sample 56B2, irradiated with 350 Gy, BSL at 25°C component analysis. The optical decay curves were deconvoluted using fit_cWCurve by (Kreutzer et al. 2024).

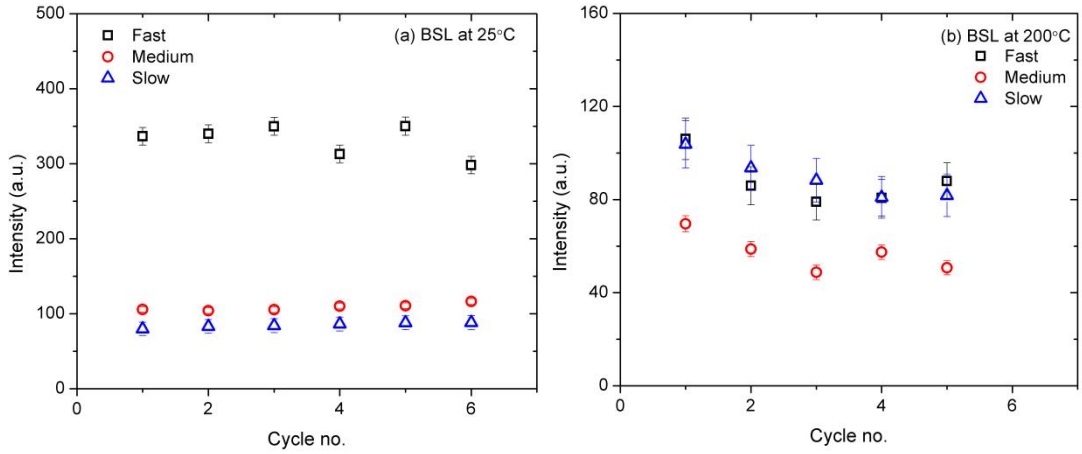

Figure S7: Sample 56B2. (a)BSL signal at 25°C. Protocol → Dose (40 Gy) → BSL at 25°C for 100 s. Repeat the protocol.(b)BSL signal at 200°C. Protocol → Dose (40 Gy) →preheat 250°C for 10 sec → BSL at 200°C for 100 s. Repeat the protocol. For reproducibility test the fast component is calculated by integrating initial 1.92 sec counts and subtracting the background from the medium component, medium by integrating 10-15 sec counts and subtracting the slow component and slow by 60-100 sec counts.

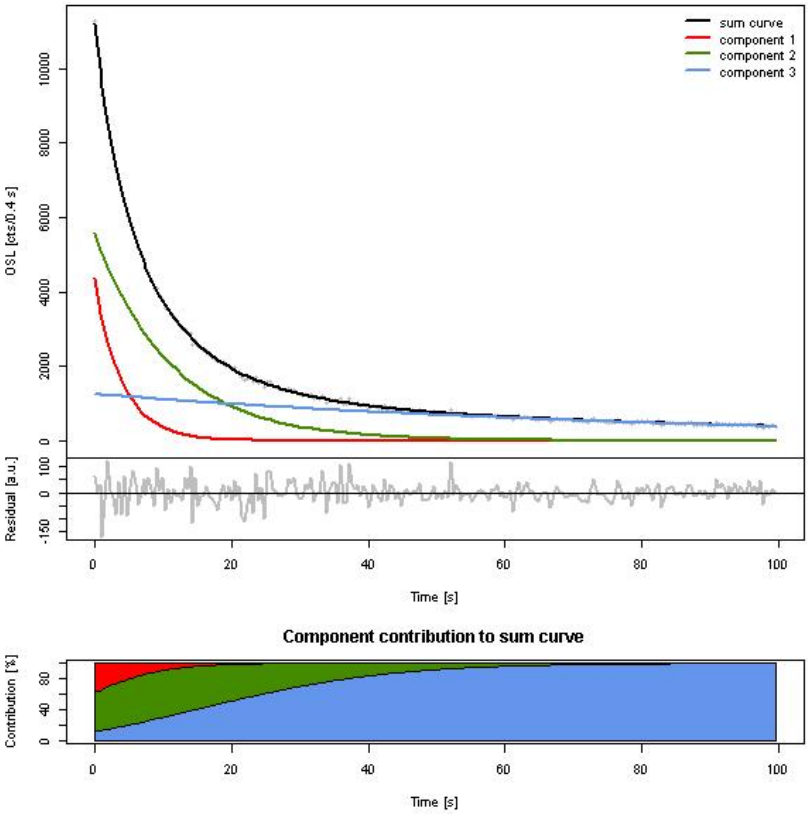

Figure S8: Sample 56B2, IRSL 50 in blue filter on a dose of 340 Gy. The optical decay curves were deconvoluted using fit_cWCurve by (Kreutzer et al. 2024).

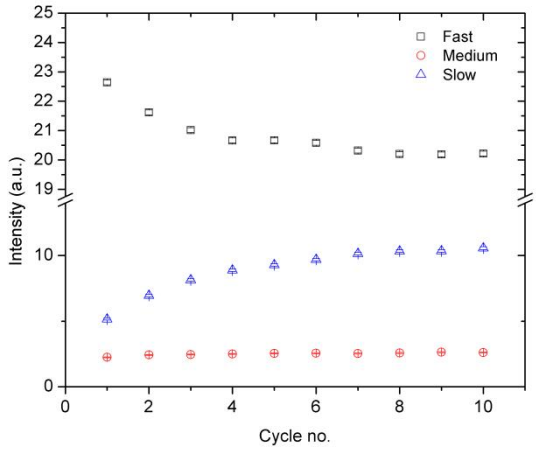

Figure S9: Sample 56B2, reproducibility of different components of the IRSL 50 signal. The fast component is calculated by integrating initial 2 sec counts and subtracting the background from the medium component, medium by integrating 35-40 sec counts and subtracting the slow component and slow by 90-100 sec counts. For more details refer to text.

References

Kerr J. B. 2005. Understanding the factors that affect surface ultraviolet radiation. *Optical Engineering* 44:41002.

Kreutzer S. et al. 2024. Package 'Luminescence.'

Patel M. R., Zarnecki J. C., and Catling D. C. 2002. Ultraviolet radiation on the surface of Mars and the Beagle 2 UV sensor. *Planetary and Space Science* 50:915–927.